Original Study **Open Access**

Phu Minh Vuong Nguyen*, Tomasz Olczak, Sywester Rajwa

An investigation of longwall failure using 3D numerical modelling – A case study at a copper mine

https://doi.org/10.2478/sgem-2021-0019
received November 25, 2020; accepted July 8, 2021.

Abstract: It is well-known that the longwall mining method (with roof caving) is widely used in underground mining extraction for bedded deposits (e.g. coal) due to its numerous advantages. Generally, this method is not commonly applied for ore deposits such as copper deposit. In Poland, the longwall mining method has been tested for thin copper deposits at the Polkowice-Sieroszowice copper mine (KGHM). Various failure modes were observed during longwall operation in the 5A/1 panel. This paper aims to examine these occurred failures. To do so, an analysis has been conducted using 3D numerical modelling to investigate the failure mode and mechanism. Based on the 3D numerical modelling results with extensive in situ measurements, causes of failure are determined and practical recommendations for further copper longwall operations are presented.

Keywords: numerical modelling; longwall mining; copper deposit; failure mechanism; back analysis.

1 Introduction

The longwall method is commonly used for regular deposit extractions (e.g. coal extraction) due to its many advantages such as small amount of preparatory work, low operational losses, high concentration of extraction, easy ground control, the possibility of full mechanisation and easy operation control in the panel. In Poland, the longwall method had been applied for copper, zinc and lead deposits earlier. The most recent longwall panel operated at the Konrad copper mine from 1965 to 1989 [1,2]. All of these ore deposit longwall operations were carried out using blasting techniques with explosive materials. They turned out unsuccessful in relation to the room–pillar method because of the low technical–economical ratio regarding the lack of possibility of fully mechanised extraction.

To date, thick and medium copper deposits in KGHM (Kombinat Górniczo-Hutniczy Miedzi) have been mined in most mining areas. With increasing depth, the remaining deposits that can be mined have reduced thickness. Where there is low deposit thickness (less than 2.0 m), room–pillar systems generate large ore impoverishment because the minimum operating height is limited by the height of operating machines. This means that more labour organisations and costs are required in relation to exploitation of medium and high deposit thickness. In addition, with the rapid advancements of technology (longwall complex with powered support and a shearer for solid rocks), the longwall method may be effective and competitive in ore mines (in relation to the room–pillar method), especially in the case of low deposit thickness [1,3].

In principle, ground control issues of longwall operation in copper deposits can be adopted from coal mining experiences. However, the significant difference in geological and mining conditions makes copper deposits an unusual case, which requires an individual analysis. Longwall operation was examined at the Polkowice-Sieroszowice copper mine in the period from 2013 to 2015 [1,2]. Roof control was the most challenging aspect during operation. Serious longwall face failures were observed at the 5A/1 longwall panel (Fig. 1). Longwall mining has been widely applied in underground coal mining for years. In order to effectively control longwall operation, numerous pieces of research have been carried out to get a better understanding of longwall face failure mechanisms. To date, two kinds of failure mechanisms of a coal wall have been put forward, that is, shear failure and tensile failure. Numerous pieces of research were conducted to analyse the factors influencing the common failure types [5–7]. Coal wall spall is a common failure phenomenon in longwall faces and usually induces roof falls, particularly when there are weak roofs or top coal (in longwall top coal caving faces) in close proximity to the worked coal seam.

***Corresponding author: Phu Minh Vuong Nguyen,** Glowny Instytut Gornictwa, Katowice, Poland, E-mail: pnguyen@gig.eu
Tomasz Olczak, KHGM Polska Miedz S.A., Polkowice-Sieroszowice mine
Sywester Rajwa, Central Mining Institute

Figure 1: Failures in the 5A/1 longwall a) roof falls, b) wall spalling.

Numerical simulation studies have shown its influence on the shape and depth of rib spalling [8–12]. Other studies were carried out to assess longwall stability and determine the interaction between the powered roof support and the rock mass [13–20].

In order to identify the 5A/1 longwall face failures, a back analysis was carried out using FLAC3D v.5 [4] by means of numerous field measurements. In this software program, two types of failure mechanisms are defined by the plasticity state plot: shear failure and tensile failure. Each type is shown with a different colour on the model plot. The model results also indicate whether stresses within a zone currently reach the yield surface or the zone failed earlier in the model run, but now the stresses drop below the yield surface. A failure mechanism is defined if there is a contiguous line of active plastic zones that join two surfaces. It is possible that initial plastic flow can occur at the beginning of calculation, but subsequent stress redistribution unloads the yielding zones, so that their stresses no longer satisfy the yield criterion. In FLAC3D, the active plastic zones will be plotted with 'n' such as shear-n or tension-n, while the passive plastic zones will be plotted with 'p' such as shear-p or tension-p.

Based on the outcomes, the main factors that caused failure at the 5A/1 longwall were defined: fracture network (natural and/or mining induced) of the rock mass around the longwall face and the tip-to-face distance. Consequently, some practical recommendations for further planned longwall operations are also suggested.

2 Case study

The Polkowice-Sieroszowice mine is a large copper mine located in the Polkowice district (west of Poland (Fig. 2).

2.1 Description of the mining technology system applied for the A5/1 longwall panel

The studied object is located in the A5 region (Fig. 3). The A5/1 longwall panel lied at an average depth of 800 m, was 2 m high and 50 m long, and the continuous mining length was approximately 240 m. The P1, P2, P3 and P4 crosscuts were driven due to the thermal hazard. The roof of the gate roads (headgate and tailgate) was supported by four 1.6-m rockbolt elements in the 1.5 × 1.5 grid. In addition, the tailgate and crosscuts (P2, P3 and P4) were reinforced by applying two 5.2-m cable elements.

Roof rocks (behind the powered roof support) were continuously deflected on to the bearing support – the LINK-N-LOCK box crib with a cross section of approximately 1 m. Cribbing was performed in a 3.5 × (4.0 ÷ 8.0) m grid (Fig. 4).

The longwall face was supported using the powered roof support presented in Figure 5.

2.2 Brief geotechnical characteristics of the rock mass in the A5 region

Copper deposit (copper seam) with an average thickness of 1.6 m (0.35 ÷ 3.2 m) and a dip of 15° contains 0.05 ÷ 0.6 m of cupriferous shale, 0.15 ÷ 0.5 m of silty dolomite, 0.8 ÷ 1.8 m of shale-streaked dolomite and 0.05 ÷ 0.8 m of limy dolomite. The roof rocks consist of dolomite, limestone and anhydrite. The floor rocks are sandstones (grey and red). The lithology of rock mass in the A5 region is shown in Table 1.

Tectonic disturbance: The rock mass in the A5 region is poorly involved tectonically. The presence of faults with small throws (0.4 ÷ 3.7 m) is confirmed. The strike line of

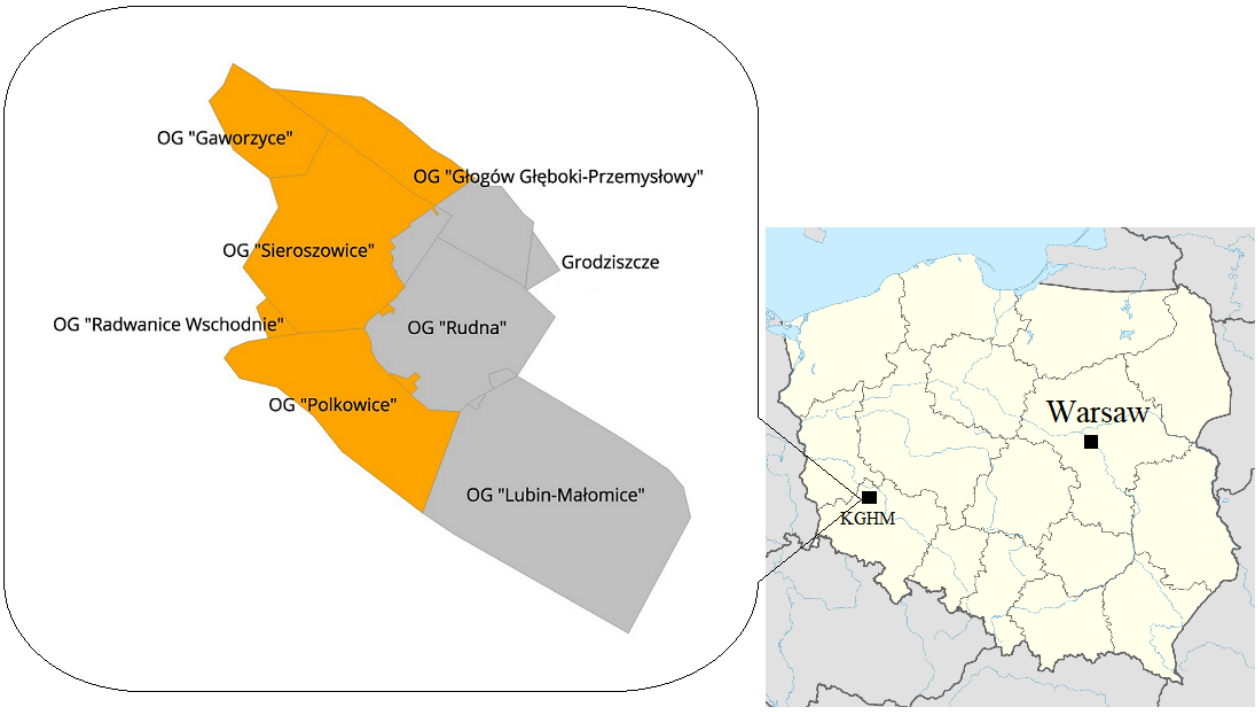

Figure 2: Location of the Polkowice-Sieroszowice copper mine.

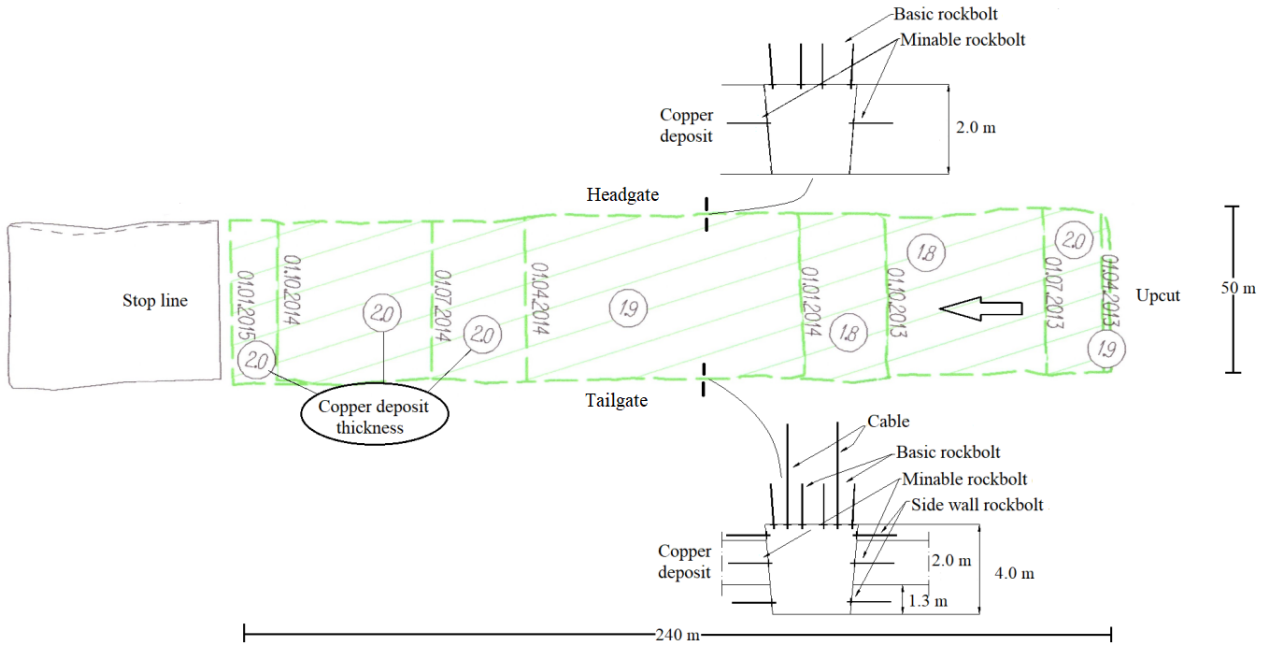

Figure 3: Outline of the A5/1 copper longwall (not to scale).

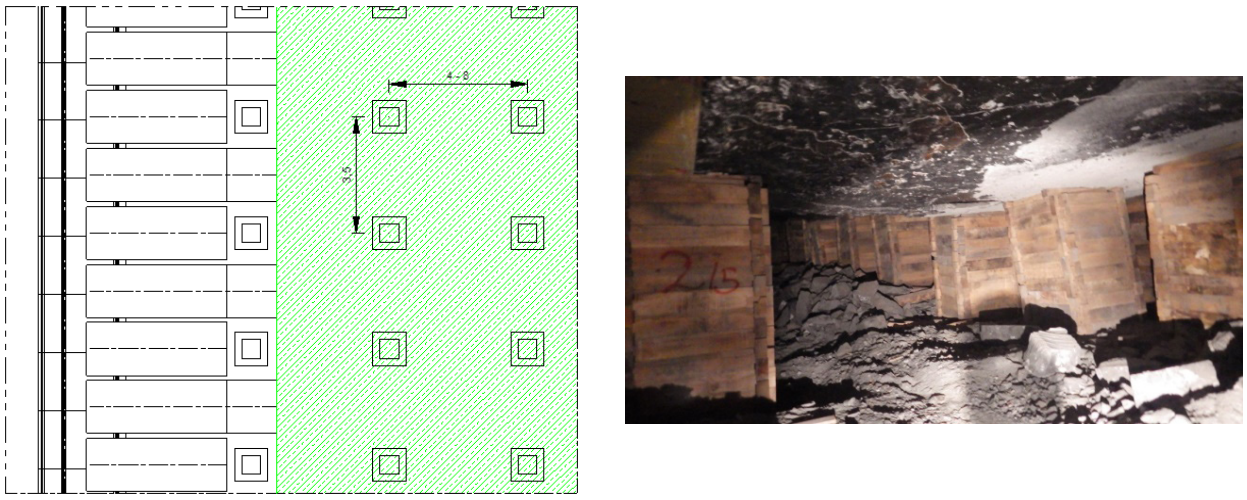

Figure 4: Spacing of box crib behind the powered roof support.

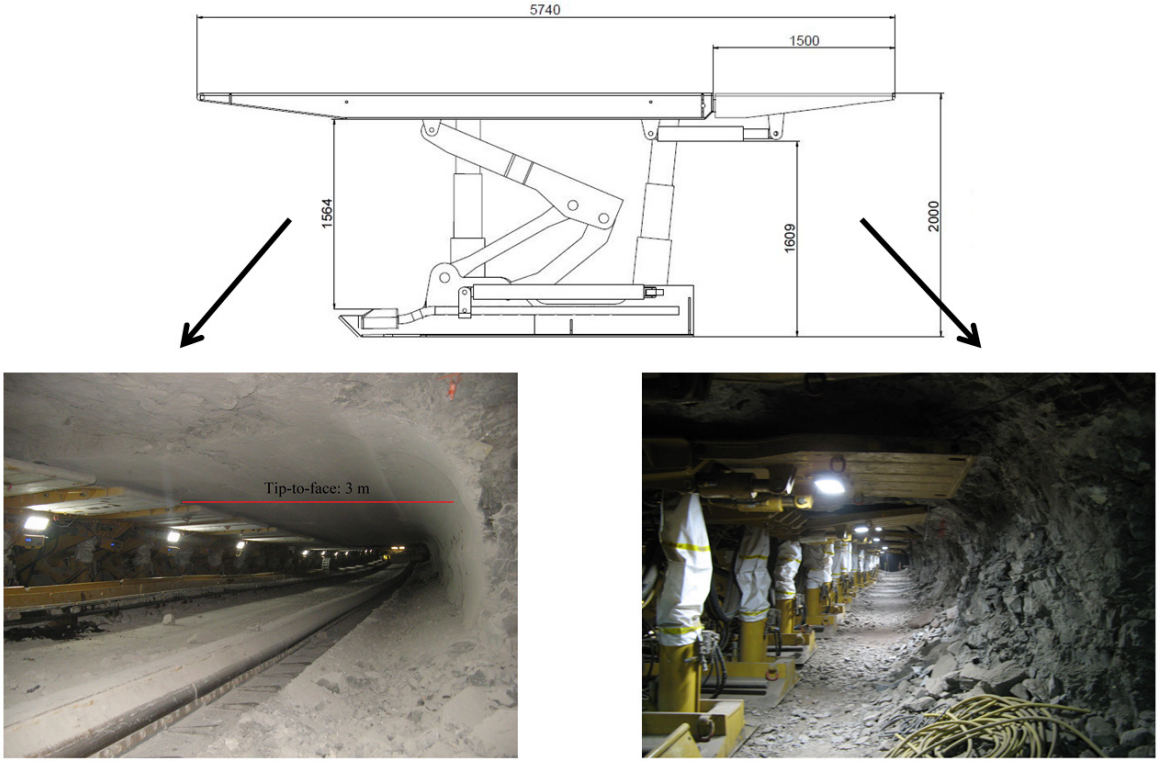

Figure 5: Outline of the powered roof support applied in the 5A/1 longwall panel at the set-up stage.

the faults is NW–SE. There are a number of vertical and skew cracks filled with gypsum and calcite. Tectonic slips occur with truncated planes of 30°.

Hydrogeological conditions: In the A5 region, carbonate rocks are strong and poorly fractured. Rock mass in the A5 region is practically unsaturated. The thick layer of impermeable anhydrite and silty shale is a separating layer against the above-lying aquifers. Traces of UG (underground) water can be found in the floor rocks (sandstones). During mining operation, the occurrence of small fluxes is possible. Larger inflows into UG workings are not anticipated.

Mechanical parameters of the intact rocks in the A5 region are shown in Table 2.

2.3 Description of the installed monitoring systems

The experimental longwall panel was subjected to 24-hour seismological monitoring. The basis for assessing the roof stability of the gate roads was regular visual observations of the state of the roof and support, as well as the side walls and floor. Visual observations were conducted once a day. In addition to visual observations of the rock mass behaviour, the following were also conducted:

1. convergence measurements in gate roads and CKN (Constrained Kohonen Network) (sensors at least twice a week),
2. geodetic measurements of the levelling of the roof in the gate roads – once a month,
3. measurements of the speed of deformation of the rocks surrounding the gate roads with a photoelectric sensor DLN (Diameter – Length) (twice a week),
4. endoscopic examination of roof in the gate roads,
5. continuous monitoring of under piston pressure of all powered roof support sections and
6. monitoring of roof rock layers using roof tilt sensors.

Photoelectric sensors (DLN-76/4/500) were used to monitor trends and the speed of rock deformation surrounding the gate roads. They measure changes in distance ΔD between the opposite walls of a borehole with a diameter of D = 76 mm and deformation ΔL of the rock along the axis of the hole relative to the base with a length of L = 500 mm. These sensors were installed in the wall sides of the tailgate at a distance of 8–10 m from the end of each mining block.

Convergence sensors (CKN-2000) were used for measuring convergence in UG workings and checking the roof deflection in gobs. These sensors measure the change in distance ΔH between the roof and floor of gate roads. These convergence sensors were installed in the middle of each cross heading between mining blocks and in gobs.

Figure 6 shows the location of convergence measuring points in the headgate (1 ÷ 14), tailgate (15 ÷ 22) and in gobs (CKN 171, CKN 173, CKN 178, CKN 176 and CKN 172). In the headgate and tailgate, distance between measuring points was about 30 m.

Table 1: Lithology of rock mass in the A5 region.

Rock mass	Rock layer thickness (m)	
Anhydrite	157	Roof rocks
Limy dolomite (I)	8	
Limy dolomite (I)	9	
Compact limy dolomite (II)	1.0	
Compact limy dolomite (II)	0.7	
Compact limy dolomite (II)	0.5	
Dolomite + shale	2.0	Copper deposit
Grey sandstone	4.4	Floor rocks
Red sandstone	200	

Table 2: Mechanical parameters of intact rocks in the A5 region.

	Bulk modulus, K (GPa)	Shear modulus, G (GPa)	Friction angle, θ (°)	Cohesion, c (MPa)	Tensile strength, R_t (MPa)	Compressive strength, R_c (MPa)	Density, γ (kg/m³)
Anhydrite	21.6	13.5	34	14.5	6.4	92.6	2950
Dolomite, limestone upper (I)	16.07	11.07	45	12.8	5.5	115.5	2750
Dolomite, limestone lower (II)	14.72	10.13	42	10.0	4.2	60.0	2650
Copper deposit	11.27	8.44	27	8.0	3.5	68.0	2600
Grey sandstone	5.12	4.32	32	5.6	2.0	37.0	2200
Red sandstone	3.72	3.36	30	4.8	1.1	25.6	1900

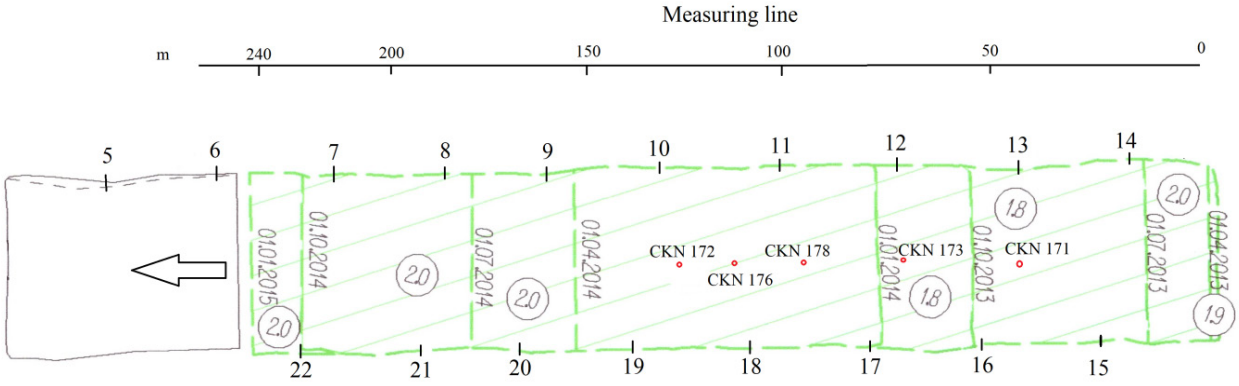

Figure 6: Location of the convergence points (not to scale).

3 Numerical modelling

3.1 Model description

Analysis of longwall failures was carried out using FLAC3D software (Itasca, 2012) [4]. The A5/1 longwall panel was modelled according to the geological and mining conditions mentioned in Section 3. Figure 7 shows the outline of the 3D numerical model and the location of the rock layers surrounding the A5/1 longwall. In all the models considered, the same block was cut out from the rock mass which is a three-dimensional deformation state. The model was divided into 632,000 elements and had dimensions of 500 m length, 250 m width and 100 m height (Fig. 7).

Hypothetically, the initial horizontal stress is equal to the vertical stress. The initial stress value was calculated by the formula presented by Biliński [21] that described the geological and mining conditions in Poland:

$$q = 0.02 \cdot H \cdot m_c \cdot \cos\alpha \tag{1}$$

where q is the primary pressure (MPa), H is the mining depth (m), m_c is a factor dependent on the geological and mining conditions of the studied site and α is the coal seam inclination (°).

For the purposes of this work, numerical calculations were carried out using the plastic model group (Mohr–Coulomb model and strain-softening model). The failure envelope for these models corresponds to the Mohr–Coulomb criterion (function of shear yield) with tension cut-off (function of tensile yield). The Mohr–Coulomb model takes into consideration the plasticity of the rock mass, which is the non-linearity of its stress–strain characteristics. The strain-softening model enables representation of non-linear material softening behaviour based on prescribed variations of the Mohr–Coulomb model properties (i.e. shear strength) as functions of the deviatoric plastic strain [4]. The plastic flow law in FLAC3D rests on basic assumptions from plasticity theory that the total strain increment may be divided into elastic and plastic parts, with only the elastic part contributing to the stress increment by means of an elastic law. In addition, both plastic and elastic strain increments are taken to be co-axial with the current principal axes of the stresses. However, this is only valid if elastic strains are small compared to plastic strains during plastic flow. The flow rule specifies the direction of the plastic strain increment vector as being normal for the potential surface; it is called associated if the potential and yield functions coincide, and non-associated otherwise [4].

The model was originally developed as an elastic model to achieve the original stress state. Then, the displacement and velocity vectors were zeroed. During the next step, the 'null' model was assigned to the zones which corresponded to the extracted copper deposit, after which support applied for the longwall panel was assigned appropriate parameters and the model was recalculated.

3.2 Modelling of the longwall support

3.2.1 Cable elements and rockbolt elements

The modelled rockbolt elements and cable elements are presented in Figure 8.

Cable element and rockbolt element properties for numerical modelling are shown in Table 3.

a

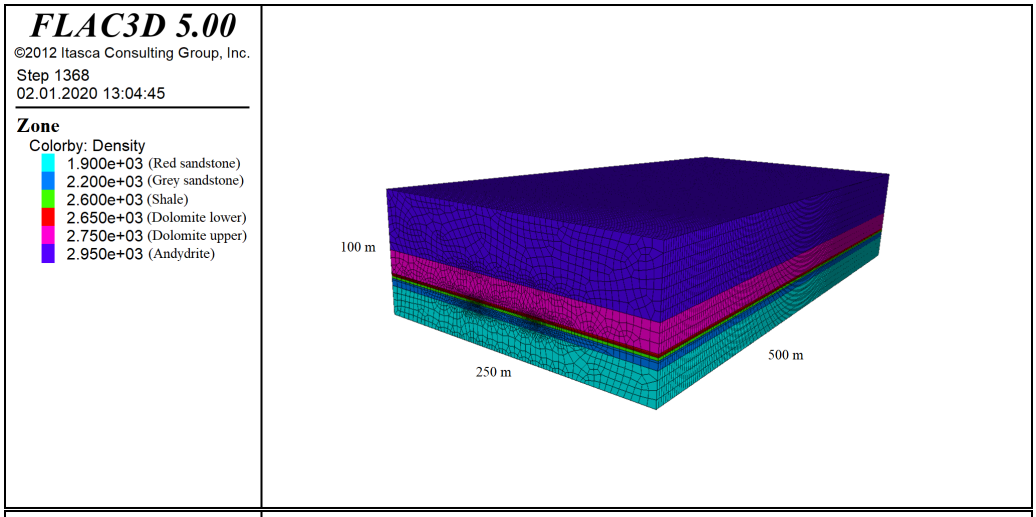

b

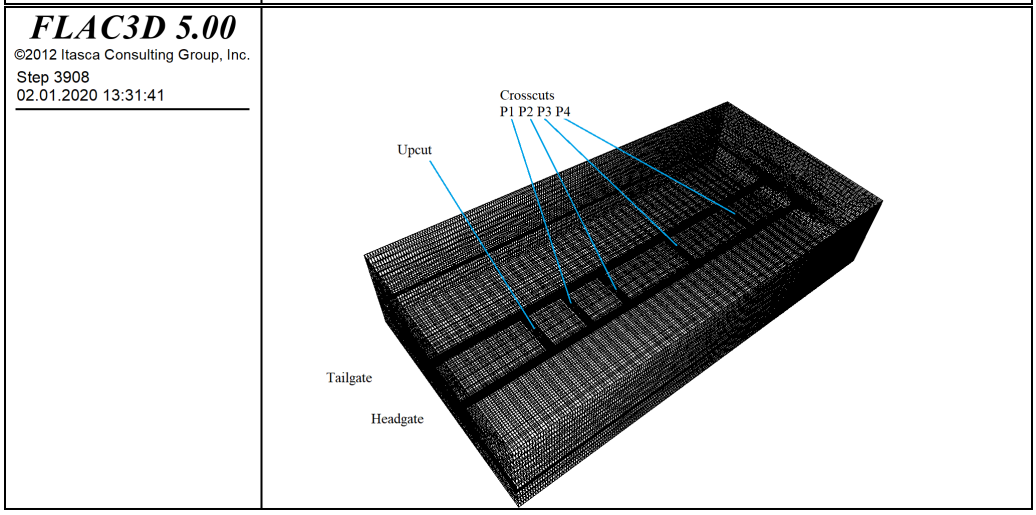

Figure 7: 3D model: a) initial model; b) outline of the 5A/1 longwall panel

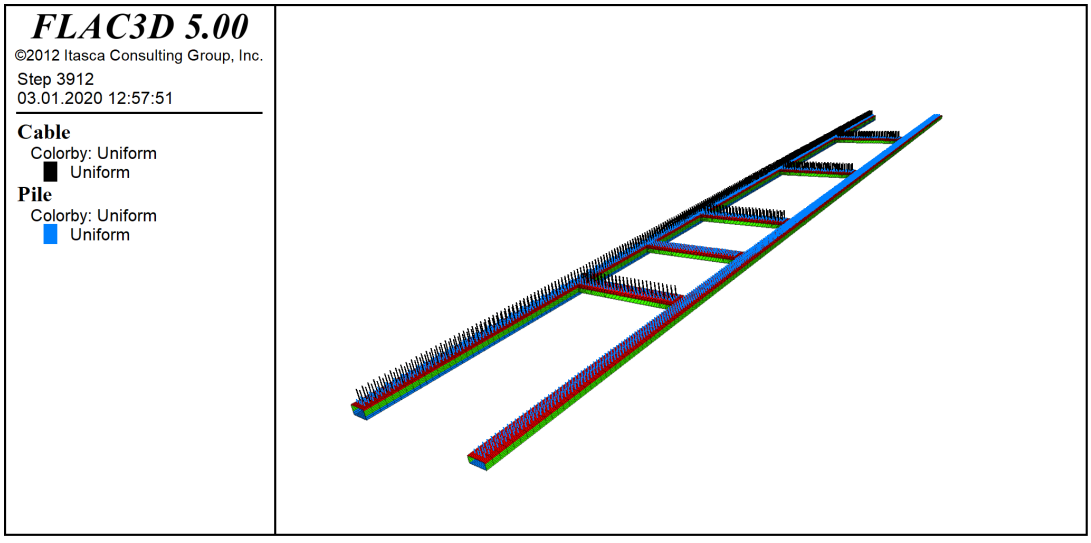

Figure 8: Cable elements (black) and rockbolt elements (blue) in a 3D model.

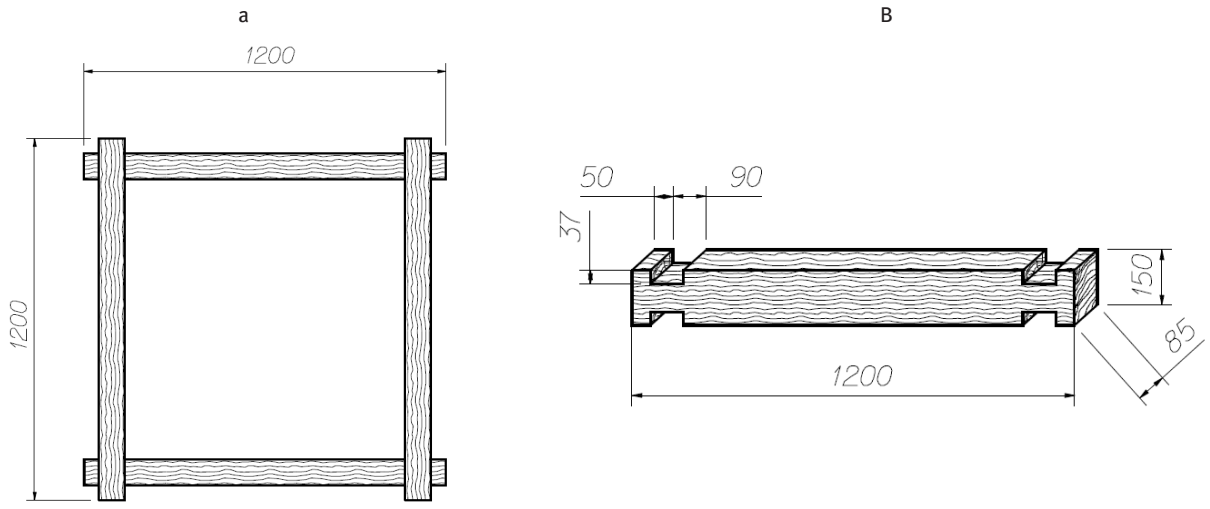

Figure 9: Sketch of the LINK-N-LOCK box crib: a) top view, b) dimensions of a single crib.

Table 3: Cable element and rockbolt element properties.

Rockbolt element		Cable element	
Rockbolt diameter, m	0.02	Cable diameter, m	0.0155
Young's modulus, GPa	200	Young's modulus, GPa	200
Cross-sectional area, m^2	3.14e-4	Cross-sectional area, m^2	1.89e-4
Exposed perimeter, m	0.063	Exposed perimeter, m	0.049
Axial tensile yield strength, N	153e3	Tensile yield strength, N	250e3
Normal coupling spring cohesion, N/m	2e6	Grout cohesive strength (force), N/m	190e3
Shear coupling spring cohesion, N/m	0.5e6	Grout stiffness, N/m/m	0.4e10
Normal coupling spring stiffness, N/m/m	1e10		
Shear coupling spring stiffness, N/m/m	40e6		

3.2.2 Box crib support

The dimensions of the LINK-N-LOCK box crib that was applied for the copper longwall are shown in Figure 9.

Figure 10 shows the characteristics of the load-bearing capacity of the LINK-N-LOCK box crib at the height of 2 m, depending on the element length. The box crib with elements of 0.8–1.5 m length provides a load capacity of 1500–2200 kN.

The load-bearing capacity of a box crib with a value of 2200 kN was adopted for modelling.

3.2.3 Powered roof support

The powered roof support shown in Figure 6 was selected and applied for the copper longwall operation. This powered roof support has two legs with an internal diameter of 200/140 mm, total canopy length of 5.74 m, coefficient of friction between the rock mass and powered support $\mu = 0.3$, operating height range of $1.0 \div 2.2$ m and width of 1.6 m. The average setting of the load-bearing capacity and the yielded load-bearing capacity are 2000 and 2600 kN, respectively. For this type of support, appropriate models were created to determine the values and distribution of the load-bearing capacity along the support canopy and the base for an operating pressure in the hydraulic legs of 32 MPa. The distribution of load-bearing capacity and its values is shown in Figure 11.

To simplify, the powered roof support was simulated in FLAC3D using a beam profile modelled with shell structural elements, including the load with values and distribution on the powered roof support canopy and base [22,15,23].

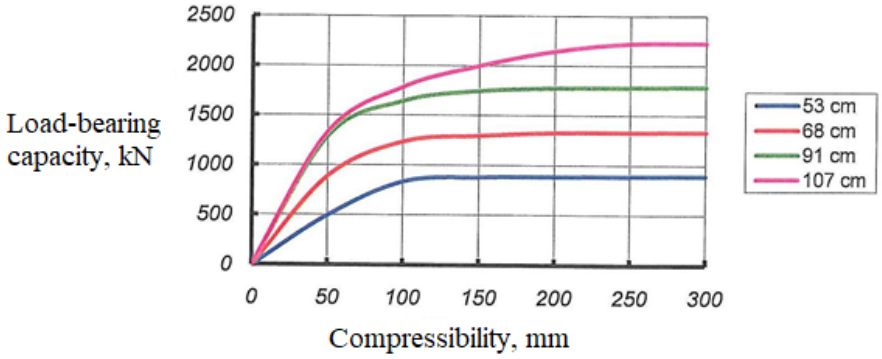

Figure 10: Load-bearing capacity of the LINK-N-LOCK box crib at the height of 2 m with different element lengths.

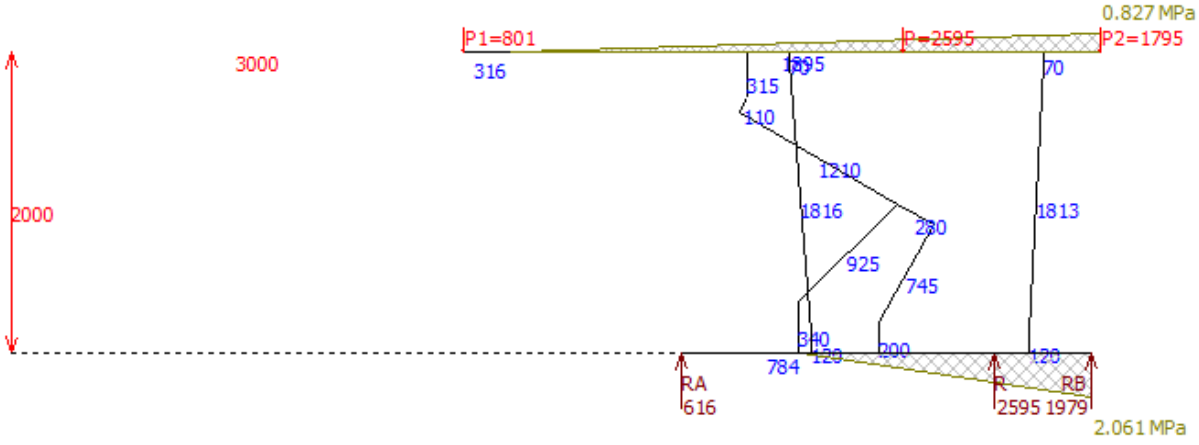

Figure 11: The value and distribution of the load-bearing capacity of the powered roof support with pressure of 32 MPa set in the hydraulic legs for an operating height of 2 m.

3.3 Geotechnical data calibration

Back analysis is a common technique for determining soil/rock properties by measuring the convergence of an underground opening. This approach has been widely applied to identify in situ stress field rock mass deformation modulus and strength parameters, rock mass hydraulic properties, rock mass zoning, boundary conditions, loads acting on tunnel linings, etc., through direct application of closed-form solutions or numerical methods [24–34]. Sakurai stated that long-term engineering experience, field measurements and back analyses are the most powerful tools in rock engineering practice [35]. Nowadays, back analysis has become an integral part of the observational method commonly used in rock engineering. To ensure excavation safety, field measurements are conducted during excavation operations to monitor possible differences between the conditions assumed in the design model and those actually observed in the field. If a difference is detected, a back analysis allows the design engineers to improve the values of the mechanical parameters of the rock and to modify, if necessary, the design or the extraction operation procedure.

Deformation monitoring data is usually used as the input data for back analysis because displacement measurements can be routinely conducted in situ and it is one of the most reliable measurable quantities in the field [24].

In this study, back analysis was conducted by matching the results of numerical modelling with the measured roof convergence as outcomes of the installed monitoring systems described in Section 3.3.

Figure 12 shows a comparison of the vertical convergence of in situ measurements and modelling results. The FLAC3D result values are close to in situ

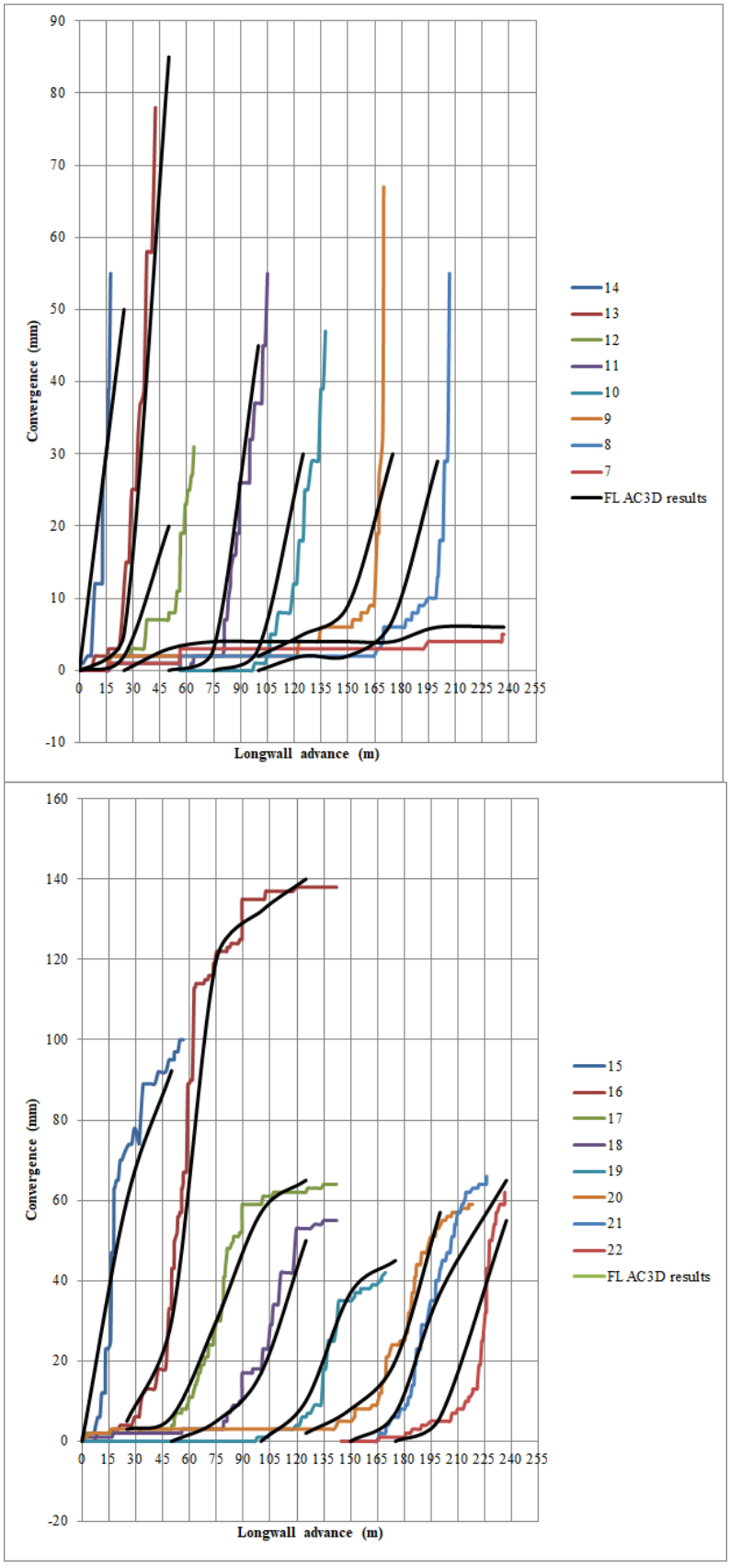

Figure 12: Progress of vertical convergence at: a) headgate, b) tailgate.

Table 4: Mechanical parameters of rock mass adopted for numerical modelling.

	Bulk modulus, K (GPa)	Shear modulus, G (GPa)	Friction angle, θ (°)	Cohesion, c (MPa)	Tensile strength, R_t (MPa)	Density, γ (kg/m³)
Anhydrite	3.60	2.25	34.0	2.40	1.10	2950
Dolomite, limestone upper	2.70	1.84	45.0	2.20	0.93	2750
Dolomite, limestone lower	2.40	1.70	42.0	1.70	0.70	2650
Copper deposit	1.80	1.40	27.0	1.35	0.60	2600
Grey sandstone	1.30	1.10	32.0	1.25	0.50	2200
Red sandstone	0.80	0.70	30.0	1.08	0.45	1900

Table 5: Mechanical parameters of rocks for the strain-softening model.

	Bulk modulus, K (GPa)	Shear modulus, G (GPa)	Friction angle, θ (°)	Cohesion, c (MPa)	Tensile strength, R_t (MPa)	Density, γ (kg/m³)	Residual friction angle, θ (°)	Residual cohesion, c_r (MPa)	Residual tensile strength, R_{tr} (MPa)
Dolomite, limestone lower	2.40	1.70	42.0	1.70	0.70	2650	32	0.7	0.15
Copper deposit	1.80	1.40	27.0	1.35	0.60	2600	22	0.35	0.10

measurements, which indicates high accuracy of the trend function match.

Based on the results of back analysis, a set of mechanical parameters that can be adopted for further numerical modelling is shown in Table 4.

3.4 Selection of the material model to simulate rock mass failure in the A5/1 longwall

The longwall face was simulated using two material models mentioned in Section 3.1 (the classic Mohr–Coulomb model and the strain-softening model). It should be noted that these strong but thin rock layers (compact limy dolomite) located immediately above the copper deposit (Table 1) behave like elastic brittle or as strain softeners. This means that the post-failure characteristics can be calculated by reducing the rock mass strength values from the in situ values [36,37]. Mechanical parameters of rocks for the strain-softening model (the assumed plastic strain parameter at the residual strength was 0.1) are shown in Table 5.

Displacement contour and failures occurred around the longwall face with the two selected material models, which are shown in Figures 13–16. The size of the failure zone and the displacement values with the strain-softening model were greater than those found using the classic Mohr–Coulomb model. In the case of the strain-softening model, both active shear and tensile failure (marked in brown, violet and blue) occurred around the longwall face. These failures were the main cause of roof falls (Fig. 15). In addition, vertical displacement in the case of strain-softening model was approximately 90 mm in the place where active tensile failure occurred (Fig. 16).

Numerical simulation results using the strain-softening model are similar to the field observations, as shown in Figures 1 and 17. This means that simulation with the strain-softening model is highly capable of characterising the behaviour of brittle rock mass and the longwall failure mechanism in such a case study. This is also confirmed by many researchers [38–42]. In the following simulation, the strain-softening model is used to analyse the impact of selected factor on longwall failures.

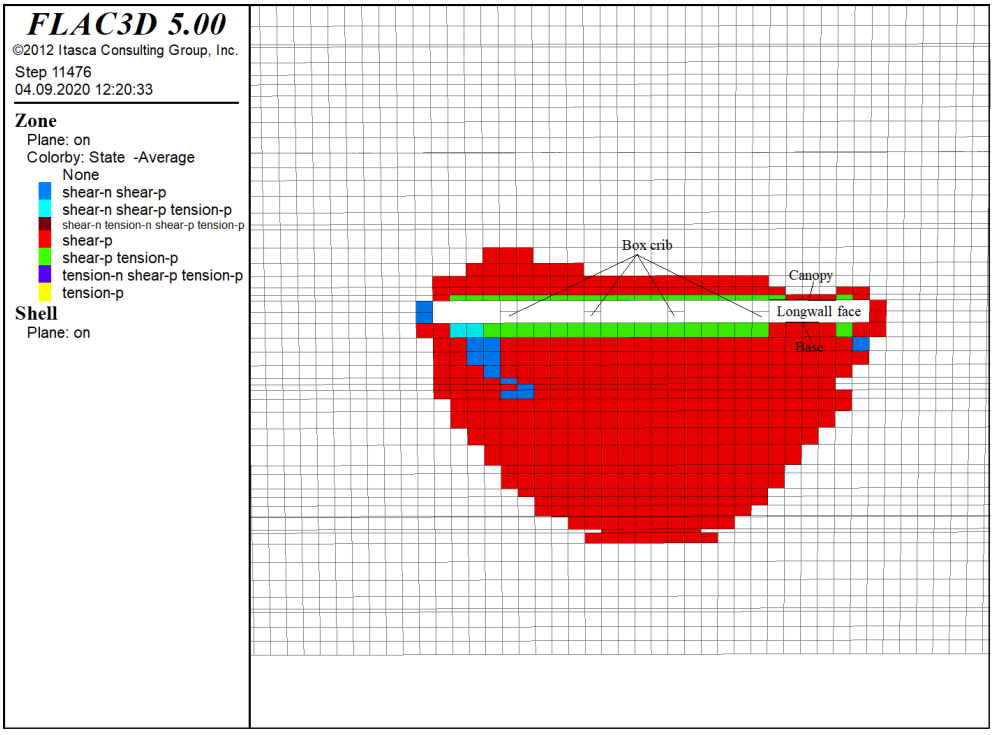

Figure 13: Failure around the longwall face using the Mohr–Coulomb model.

Table 6: Numerical calculation scenarios.

Factor	Original designed parameters	Modified parameters
Tip-to-face distance	3.0 m	1.5 m
Average load-bearing capacity	2600 kN	4000 kN
Spacing of box crib	Every 6.0 m	Every 3.0 m, 1.5 m
Roof control method – hydraulic backfilling (sand) instead of box crib	No	Yes

3.5 Modelling variations

Based on the geological and mining conditions in the 5A region, different operating factors were considered in order to investigate the longwall face failures and prevent those failures from threatening the future copper longwall operation. These different operating factors were: tip-to-face distance, load-bearing capacity of the powered roof support, spacing of the box crib and the roof control method. Therefore, different scenarios were used as shown in Table 6.

4 Results analysis and discussion

Due to the large number of obtained results, only selected maps for certain calculation variations are presented in this article.

4.1 Impact of the tip-to-face distance

The plasticity indicator around the longwall face with different tip-to-face distances is shown in Figure 18.

It should be noted that shear failure only occurred in the case of tip-to-face distance of 1.5 m, while in the case of tip-to-face distance of 3 m, both shear and tensile failures of rock mass occurred around the longwall face, in contact with the powered roof support canopy. This means that the possibility of roof rock falls when there is a 3-m-long tip-to-face distance is higher than that when there is a 1.5-m-long tip-to-face distance.

4.2 Impact of the box crib spacing

The plasticity indicator around the longwall face with different box crib spacing is shown in Figure 19. The size of the failure zone above the longwall panel decreased

a

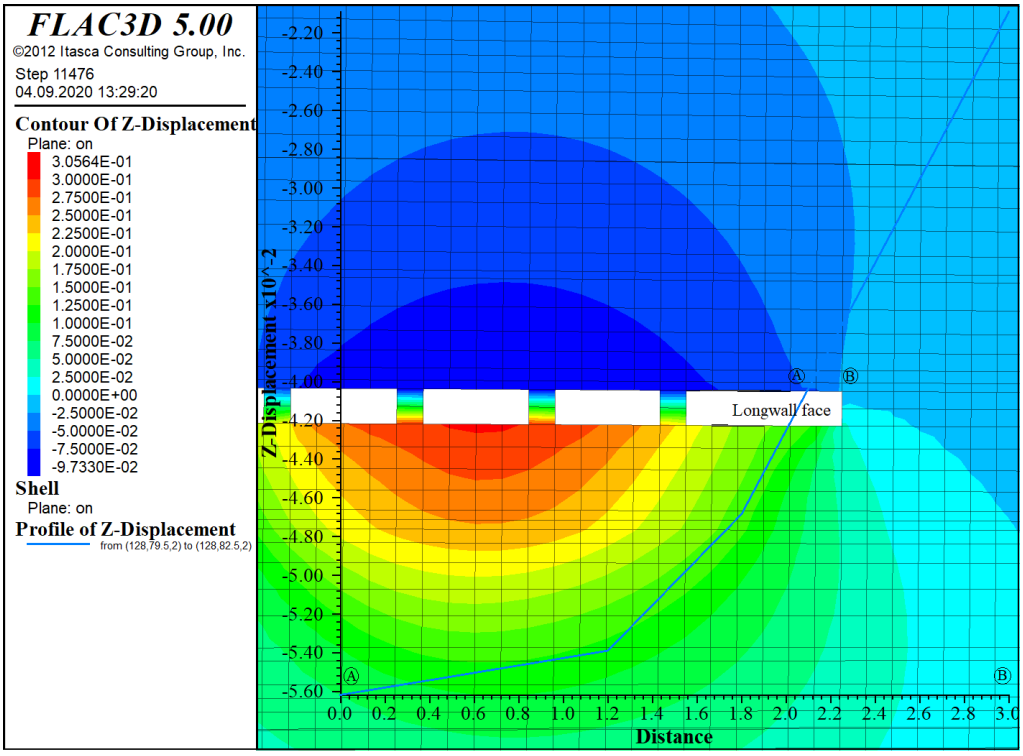

b

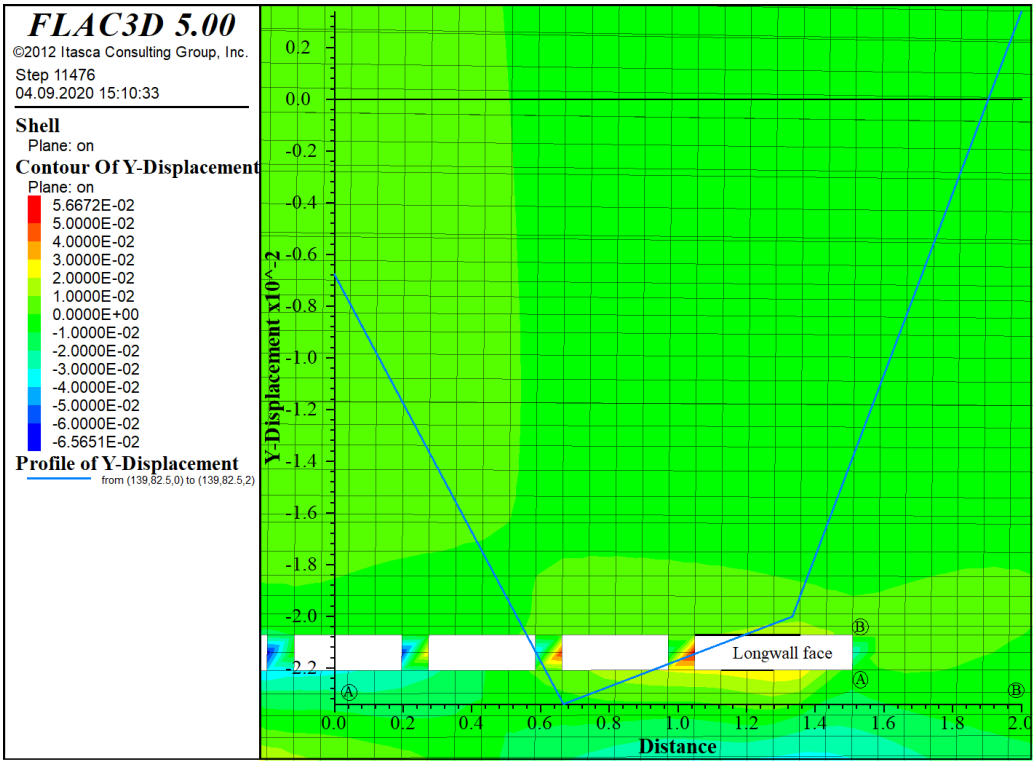

Figure 14: Displacement around the longwall face using the Mohr–Coulomb model: a) vertical displacement along the tip-to-face distance, b) horizontal displacement along the longwall face.

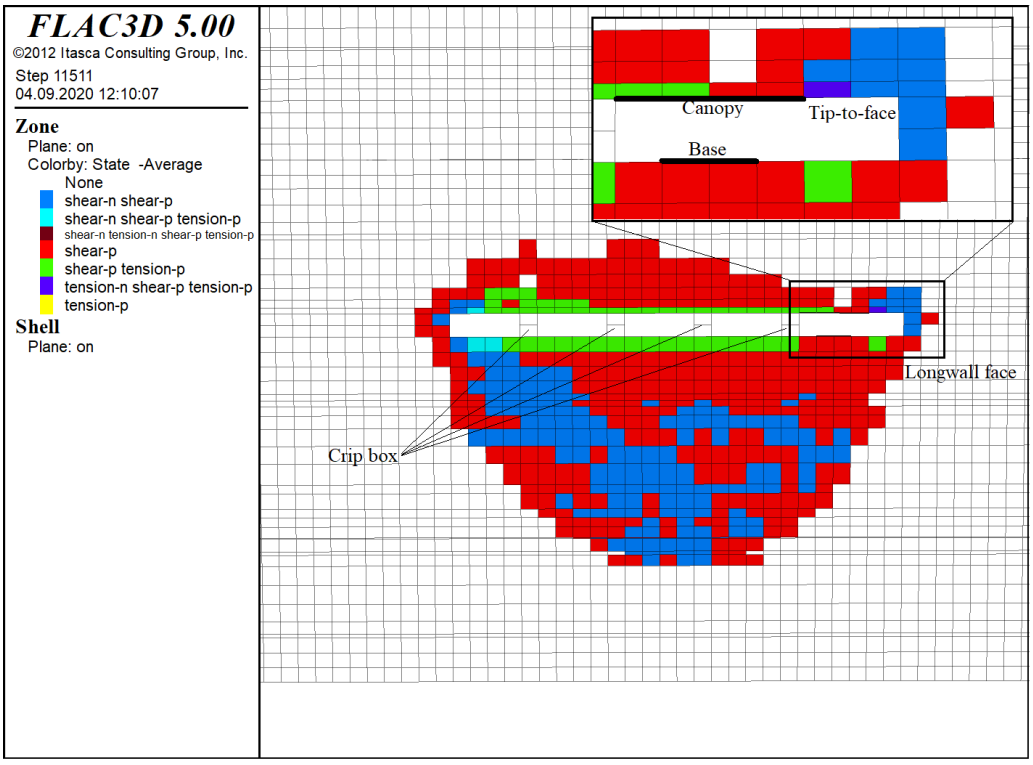

Figure 15: Failures around the longwall face using the strain-softening model.

due to the reduction of box crib spacing. Both active shear and tensile failures occurred in the case of 6-m box crib spacing (Fig. 19a). In the case of 1.5- and 3-m box crib spacing, only active shear failure occurred around the longwall face (Fig. 19b, c).

4.3 Impact of the hydraulic backfilling

In mining practice, backfilling is considered to be the best option when it comes to improving the roof conditions. In the case of applying backfilling (e.g. sand), the size of the failure zone around the longwall panel decreased significantly. The size of the active failure zone around the longwall face also decreased (Fig. 20). Both roof and floor rocks behind the powered roof support will be evenly deflected in lower scale in comparison with the case of applying box crib (Fig. 19). Backfilling aims to minimise displacement of roof and floor rocks to the mined space. In consequence, it prevents failures around the longwall.

4.4 Impact of the load-bearing capacity of the powered roof support

Figure 21 shows the plasticity indicator around the longwall face with different operating load-bearing capacities of the powered roof support. The size of the active shear and tensile failure zone decreased with higher load-bearing capacities. This means that an increase in the load-bearing capacity improves the roof conditions.

4.5 Impact of the selected factors combined

A simulation with lower tip-to-face distance (1.5 m), higher load-bearing capacity of the powered roof support (4000 kN) and lower spacing of the box crib (1.5 m) was conducted. The results showed that the size of the failure zone above the longwall panel decreased in comparison to the originally designed case, as shown in Figures 18a, 19a and 21a. In addition, the active failure zone around the longwall face also decreased significantly (Fig. 22). This means that changes in the selected factors combined clearly improve the roof conditions, avoiding possible failure around the longwall face.

a

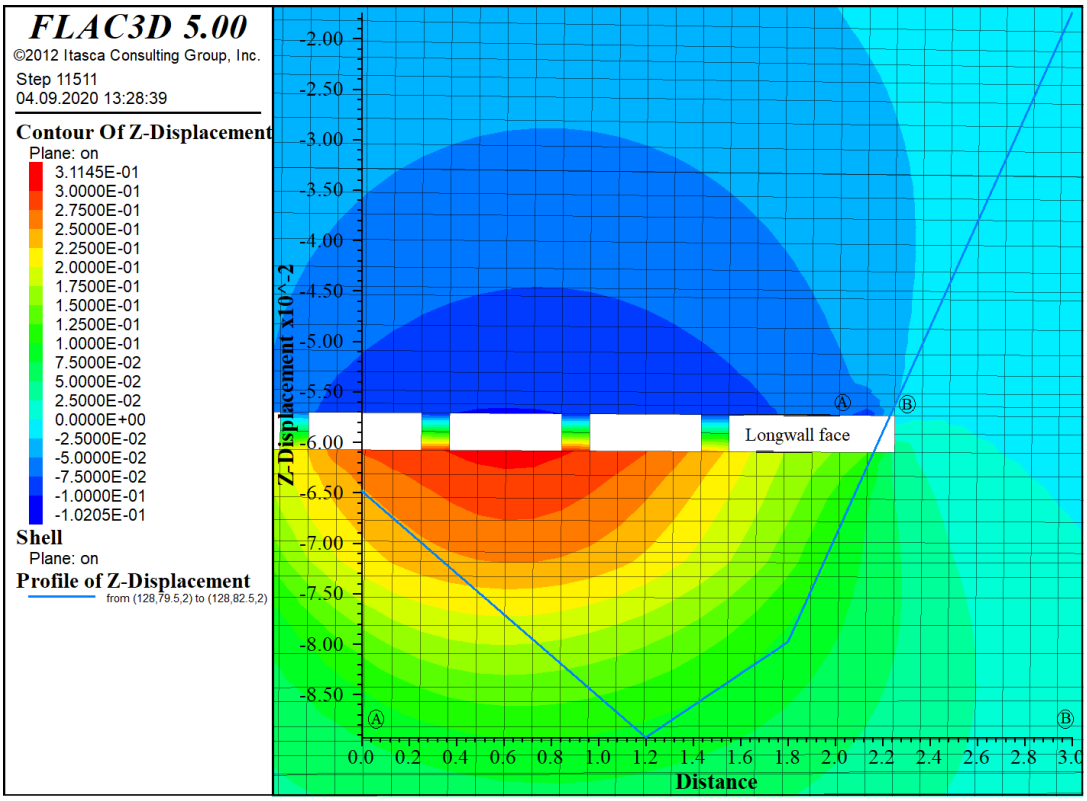

b

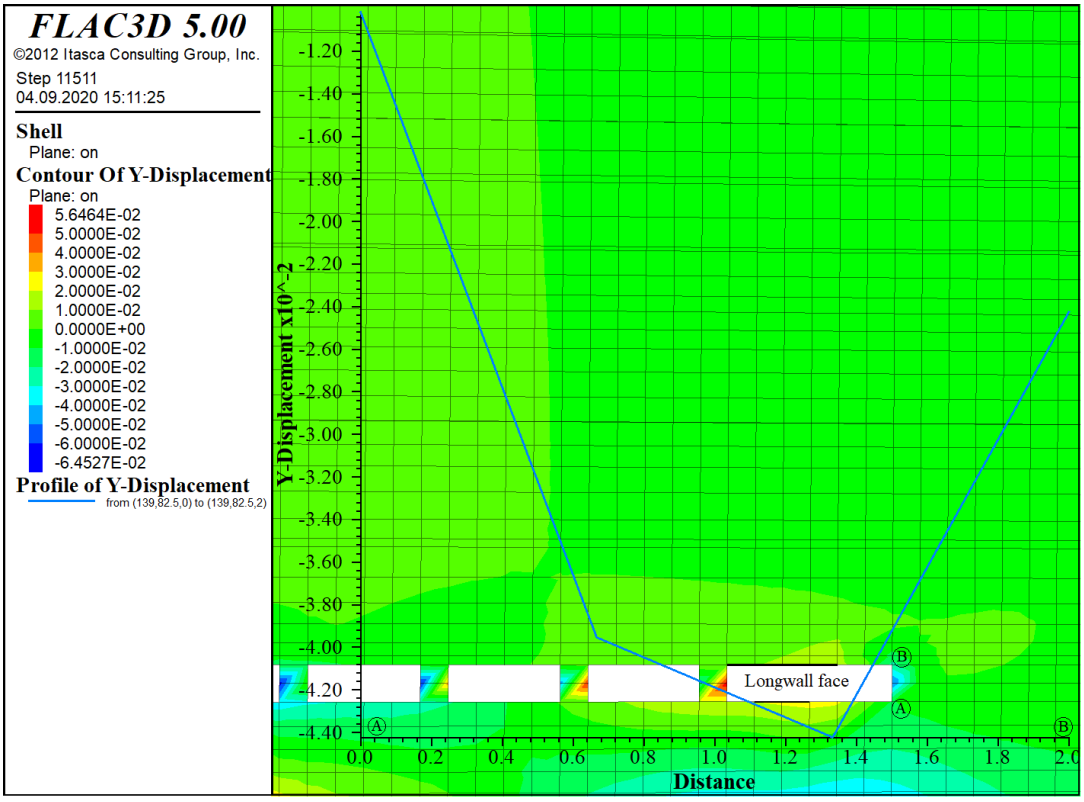

Figure 16: Displacement around the longwall face using the strain-softening model: a) vertical displacement along the tip-to-face distance, b) horizontal displacement along the longwall face.

a

b

C

Figure 17: Examples of failures that occurred in the 5A/1 longwall: a, b) roof falls, c) wall spalling.

A

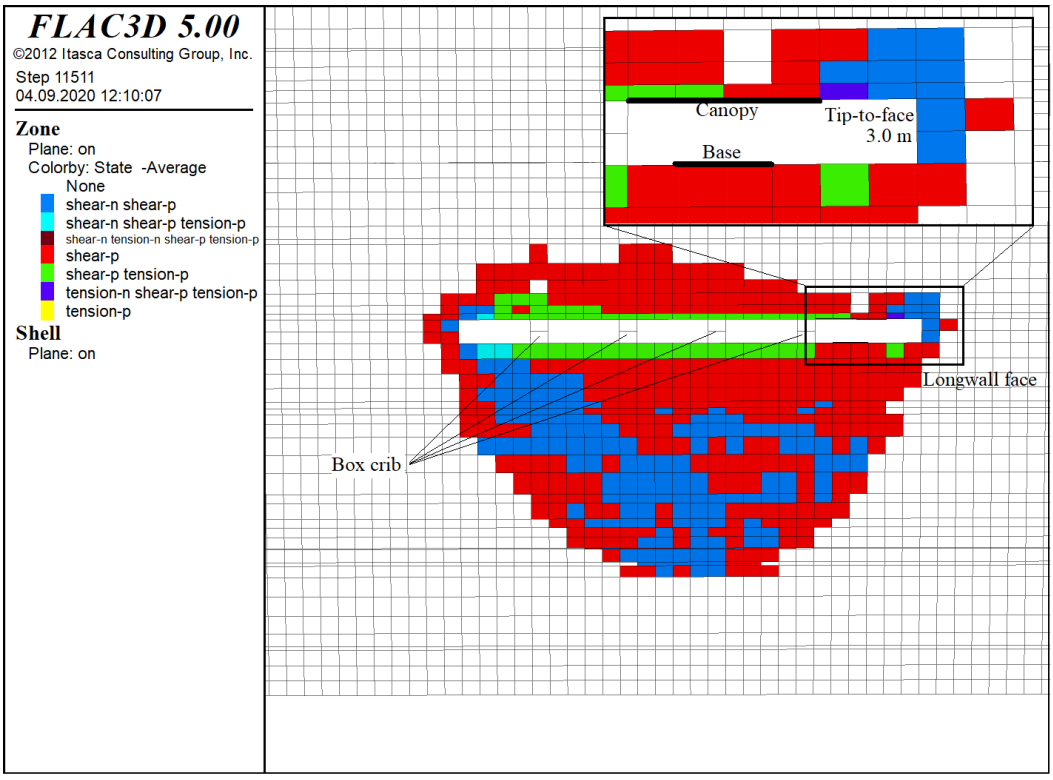

b

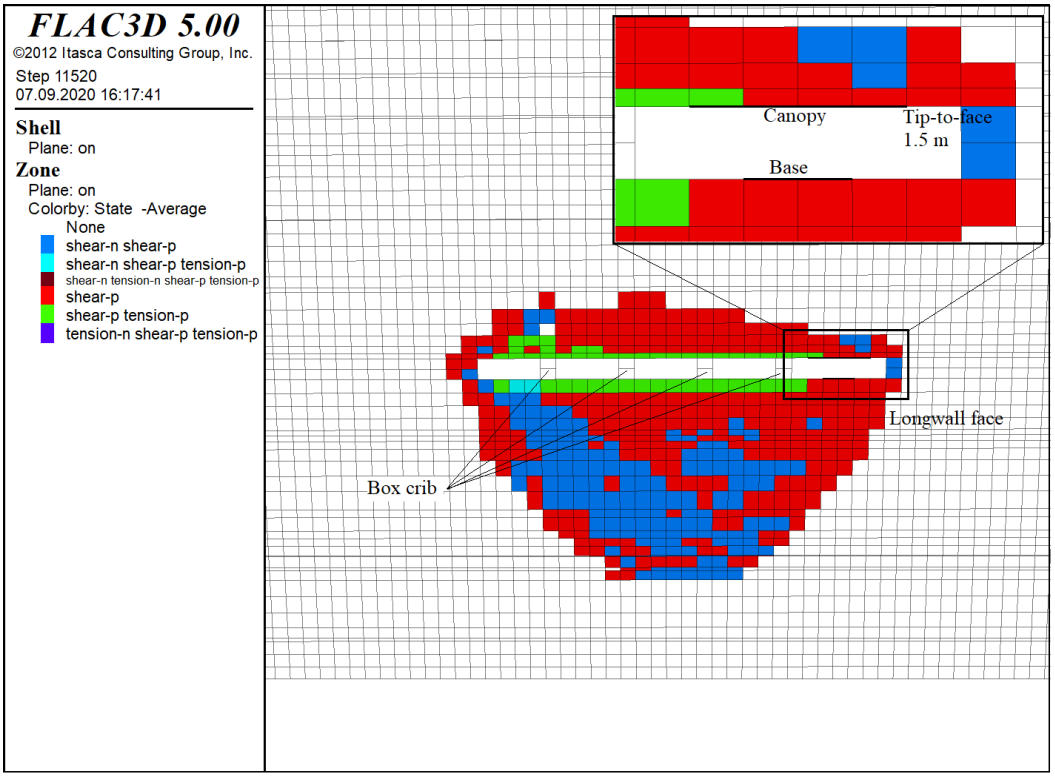

Figure 18: Plasticity around the longwall face with a) tip-to-face distance of 3 m, b) tip-to-face distance of 1.5 m.

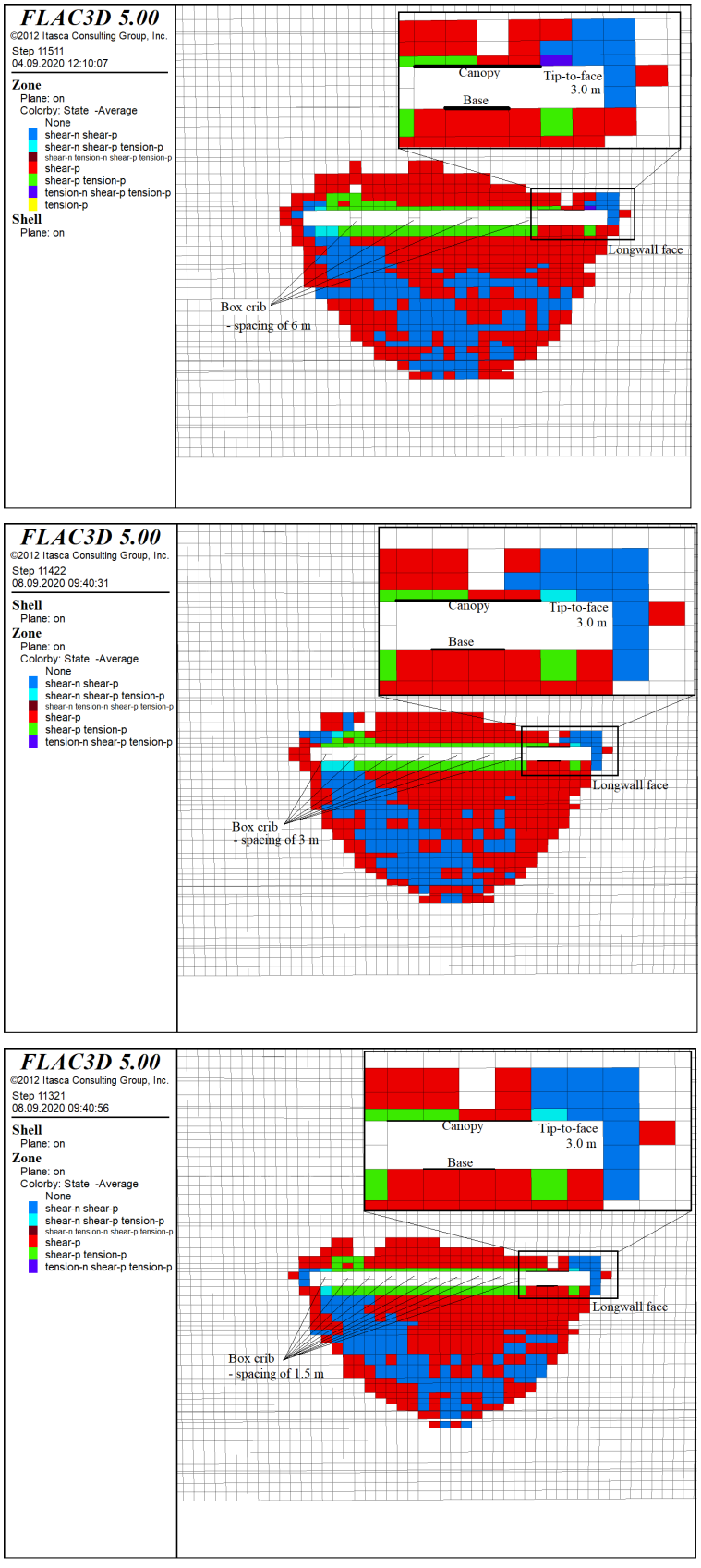

Figure 19: Plasticity around the longwall face with different spacing of the box crib: a) 6.0 m, b) 3.0 m and c) 1.5 m.

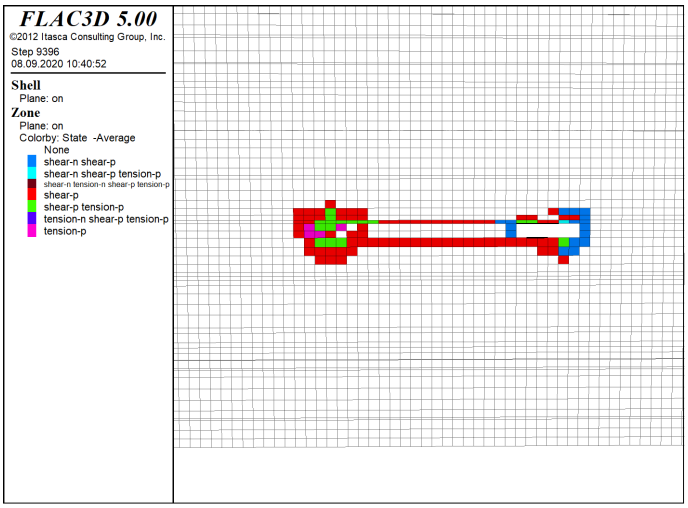

Figure 20: Plasticity around the longwall face with hydraulic backfilling (sand).

a

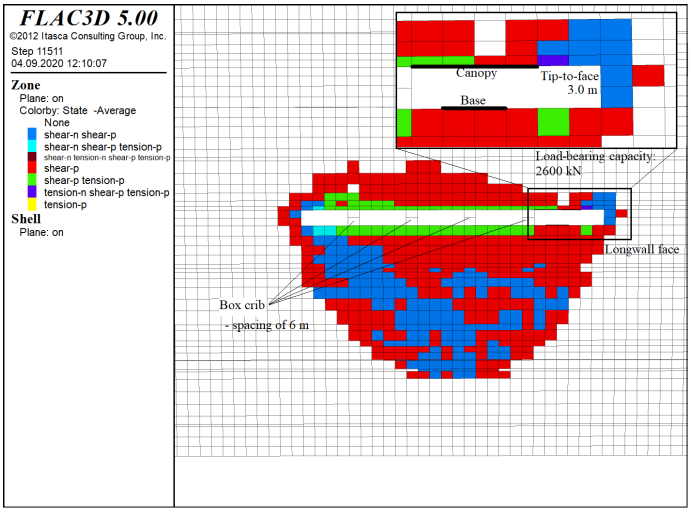

b

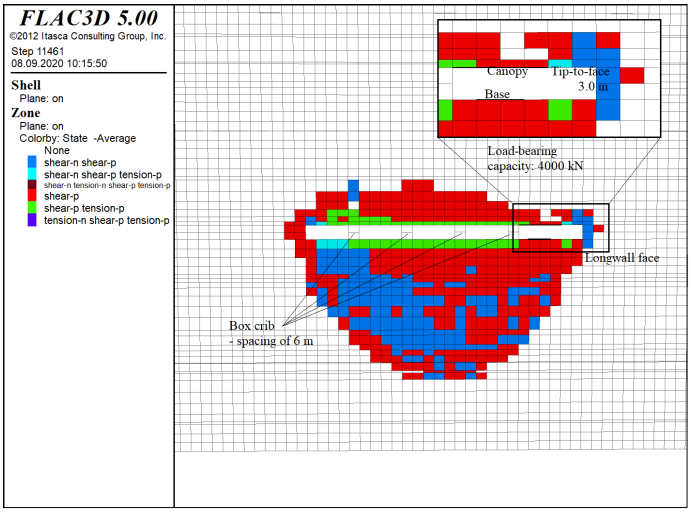

Figure 21: Plasticity around the longwall face with different load-bearing capacities of the powered roof support: a) 2600 kN b) 4000 kN.

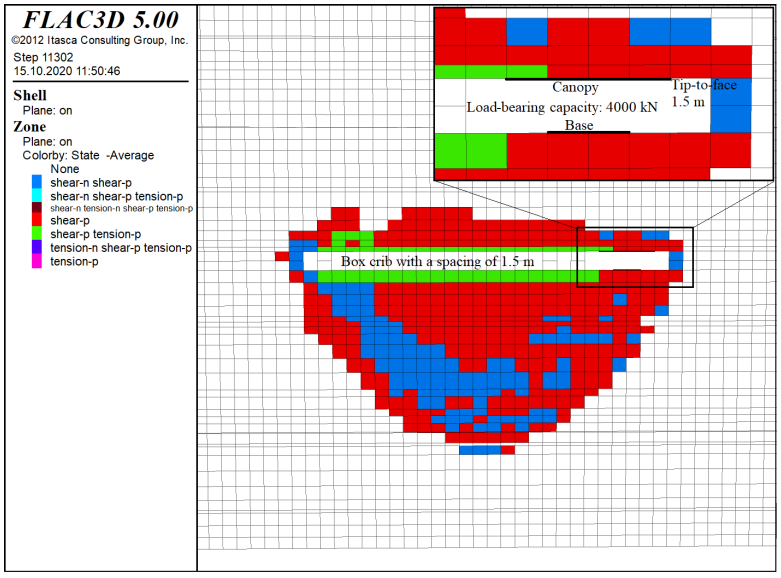

Figure 22: Plasticity around the longwall face with the selected influencing factors combined.

5 Conclusions and recommendations

In this study, 3D numerical analysis was conducted in order to investigate the failure that occurred in the copper longwall panel in the Polkowice-Sieroszowice mine (KGHM). A series of factors that possibly impact longwall working stability were taken into consideration. The numerical results coupled with the in situ measurements allowed the following conclusions to be made:

1. The main natural factor that causes failure is the fracture network (natural and/or mining induced) of the rock mass around the longwall face. Moreover, greater tip-to-face distance (3 m) associated with the fractures of roof rock also cause failure.
2. Based on the results from numerical modelling, some suggestions can be proposed in order to improve the roof conditions and prevent failures in the copper longwall: (a) reduction of the tip-to-face distance; (b) densification of the box crib behind the powered roof support or application of hydraulic backfilling and (c) application of higher load-bearing capacity for the powered roof support. All the aforementioned actions are commonly used in coal mining practices in order to improve the roof conditions of a longwall face.
3. Based on coal mining practices, it is suggested that stoppage time and the number of crosscuts in the front of the longwall face should be reduced. Both actions cause the concentration of vertical stress on the longwall face. Consequently, failures occur around the longwall face.
4. It is also suggested that research regarding rock mass classification and the fracture network should be carried out, the outcomes of which can lead to achievement of greater accuracy and reliability of numerical analysis results.
5. This study proves that using the strain-softening model is a proper approach for simulating brittle failures such as those that occur in the analysed copper mine.
6. In this study, a selected series of geological and mining factors can be simultaneously taken into account, which is impossible in analytical and/or empirical analyses. This, once again, confirms that modelling is a helpful tool for solving complex geotechnical problems, especially when coupled with the results of laboratory tests and in situ tests.

References

[1] Butra J, Dębkowski R, Matusz C, Serafin M. Research on the behavior of the rock mass during the experimental exploitation with the longwall method in the A5/1, Polkowice-Sieroszowice copper mine. CUPRUM – Scientific and Technical Journal of Ore Mining, V. 1 (74) 2015, pp. 23-40 (in Polish).

[2] Konopko W, Piernikarczyk A. Concept of the extraction technology for thin copper deposits. CUPRUM – CUPRUM – Scientific and Technical Journal of Ore Mining, V. 4 (73) 2014, pp. 17-33 (in Polish).

[3] Ziętkowski L, Młynarczyk J. Mechanical mining of hard rock using shearer in the KGHM copper mines. Inżynieria Maszyn 2014, V 19 (2) (in Polish).
[4] FLAC3D, Version 5.0, Itasca Consulting Group Inc., Minneapolis (2012); software available at www.itascacg.com.
[5] Wang JC, Wang ZH. Systematic principles of surrounding rock control in longwall mining within thick coal seams. Int. J. of Min. Sci. and Technol. 2018. V. 29 (1), pp. 65-71. DOI: 10.1016/j.ijmst.2018.11.014.
[7] Wang JC, Yang SL, Kong DZ. Failure mechanism and control technology of longwall coalface in large-cutting-height mining method. Int. J. Min. Sci. Technol. 2015, 26 (1), pp. 111-118. DOI: 10.1016/j.ijmst.2015.11.018.
[8] Bai QS, Tu SH, Li ZX, Tu HS. Theoretical analysis on the deformation characteristics of coal wall in a longwall top coal caving face. Int. J. Min. Sci. Technol. 2015, 25 (2), pp. 199-204. DOI: 10.1016/j.ijmst.2015.02.006.
[9] Bai QS, Tu SH, Chen M, Zhang C. Numerical modelling of coal wall spall in a longwall face. Int. J. of Rock Mech. and Min. Sci. 2016, V. 88, pp. 242-253. DOI: 10.1016/j.ijrmms.2016.07.031.
[10] Li XM, Wang ZH, Zhang JW. Stability of roof structure and its control in steeply inclined coal seams. Int. J. Min. Sci. Technol. 2017, 27 (2), pp. 359-364. DOI: 10.1016/j.ijmst.2017.01.018.
[11] Xin YJ, Gou PF, Ge FD. Analysis of stability of support and surrounding rock in mining top coal of inclined coal seam. Int. J. Min. Sci. Technol. 2014, 24 (1), pp. 63-68. DOI: 10.1016/j.ijmst.2013.12.011.
[12] Prusek S, Rajwa S, Wrana A, Krzemień A. Assessment of roof fall risk in longwall coal mines, International Journal of Mining, Reclamation and Environment 2017, 31:8, 558-574. DOI: 10.1080/17480930.2016.1200897.
[13] Masny W. Powered support in dynamic load conditions – numerical analysis. Archives of Mining Sciences 2020, Vol. 65 No 3, s.453-468. DOI: 10.24425/ams.2020.134129.
[14] Islavath SR, Deb D, Kumar H. Life cycle analysis and damage prediction of a longwall powered support using 3D numerical modelling techniques. Arab. J. of Geosci. 2019, 12:441. DOI: 10.1007/s12517-019-4574-y.
[15] Rajwa S, Janoszek T, Prusek S. Influence of canopy ratio of powered roof support on longwall working stability – A case study. Int. J. of Min. Sci. and Technol. 2019, 29(4). DOI: 10.1016/j.ijmst.2019.06.002.
[16] Witek M, Prusek S. Numerical calculations of shield support stress based on laboratory test results. Computers and Geotechnics 2016, 72:74-88. DOI: 10.1016/j.compgeo.2015.11.007.
[17] Bai QS, Tu SH, Zhang XG. Numerical modelling on brittle failure of coal wall in longwall face – a case study. Arab. J. Geosci. 2014, 7: 5067-5080. DOI: 10.1007/s12517-013-1181-1.
[18] Verma AK, Deb D. Numerical Analysis of an Interaction between Hydraulic-Powered Support and Surrounding Rock Strata. Int. J. of Geomech. 2013, V. 13 (2). DOI: 10.1061/(ASCE)GM.1943-5622.0000190.
[19] Singh GSP, Singh UK. Prediction of caving behaviour of strata and optimum rating of hydraulic powered support for longwall workings. Int. J. of Rock Mech.and Min. Sci. 2010, 47(1): 1-16. DOI: 10.1016/j.ijrmms.2009.09.001.
[20] Trueman R, Lyman G, Cocker A. Longwall roof control through a fundamental understanding of shield–strata interaction. International Journal of Rock Mechanics and Mining Sciences 2009, 46(2): 371-380. DOI: 10.1016/j.ijrmms.2008.07.003.
[21] Biliński A. Method of selection of longwall face and roadway supports for the panelling conditions; 2005.
[22] Janoszek T. The Assessment of longwall working stability based on the Mohr-Coulomb stress criterion – Numerical Analysis. Archives of Mining Sciences 2020, V. 65 (3), pp. 493-509. DOI: 10.24425/ams.2020.134131.
[23] Song G, Chugh YP, Wang J. A numerical modelling study of longwall face stability in mining thick coal seams in Chin. Int. J. Mining and Mineral Engineering 2017, Vol. 8, No. 1, pp.35–55. DOI: 10.1504/IJMME.2017.10003216.
[24] Cai M, Morioka H, Kaiser PK, Tasaka Y, Kurose H, Minami M, Maejima T. Back-analysis of rock mass strength parameters using AE monitoring data. Int. J. of Rock Mech. and Min. Sci. 2007, V. 44 (4), pp. 538-549. DOI: 10.1016/j.ijrmms.2006.09.012.
[25] Gioda G, Sakurai S. Back-analysis procedures for the interpretation of field measurements in geomechanics. Int. J. Numer. Anal. Methods Geomech., 1987, 11, pp. 555-583. DOI: 10.1002/nag.1610110604.
[26] Kaiser PK, Zou D, Lang PA. Stress determination by back-analysis of excavation-induced stress changes—a case study. Rock Mech. Rock Eng. 1990, 23 (3), pp. 185-200. DOI: 10.1007/BF01022953.
[27] Sakurai S, Akutagawa S, Takeuchi K, Shinji M, Shimizu N. Back-analysis for tunnel engineering as a modern observational method. Tunnelling Underground Space Technology. 2003, 18 (2), pp. 185-196. DOI: 10.1016/S0886-7798(03)00026-9.
[28] Ceryan N, Kesimal A, Ceryan S. Chapter 13 - Probabilistic Analysis Applied to Rock Slope Stability: A Case Study From Northeast Turkey. Integrating Disaster Science and Management Global Case Studies in Mitigation and Recovery 2018 Ed. P. Samui, D. Kim, C. Ghosh, pp. 221-261.
[29] Bakhtiyari E, Almasi A, Cheshomi A, Hassanpour J. Determination of Shear Strength Parameters of Rock Mass using Back Analysis Methods and Comparison of Results with Empirical Methods. EJERS, European Journal of Engineering Research and Science 2017, Vol. 2, No. 11. DOI: 10.24018/ejers.2017.2.11.518.
[30] Kim YT, Lee SR. An equivalent model and back-analysis technique for modelling in situ consolidation behavior of drainage-installed soft deposits. Computers and Geotechnics 1997, Volume 20, Issue 2, pp. 125-142. DOI:10.1016/S0266-352X(96)00016-X.
[31] Wu Y, Yuan H, Zhang B, Zhang Z, Yu Y. Displacement-Based Back-Analysis of the Model Parameters of the Nuozhadu High Earth-Rockfill Dam. Scientific World Journal 2014, No: 292450. DOI: 10.1155/2014/292450.
[32] Fakhimi A, Salehi D, Mojtabai N. Numerical back analysis for estimation of soil parameters in the Resalat Tunnel project. Tunnelling and Underground Space Technology 2004, 19(1):57-67. DOI: 10.1016/S0886-7798(03)00087-7.
[33] Pu Y, Apel DB, Prusek S, Walentek A, Cichy T. Back-analysis for initial ground stress field at a diamond mine using machine learning approaches. Nat. Hazards 2020. DOI: 10.1007/s11069-020-04304-1.
[34] Cichy T, Prusek S, Świątek J, Apel D, Pu Y. Use of Neural Networks to Forecast Seismic Hazard Expressed by Number of

Tremors Per Unit of Surface. Pure Appl. Geophys., 2020. DOI: 10.1007/s00024-020-02602-0.
[35] Sakurai S. Back analysis in Rock Engineering. International society for Rock mechanics. ISRM book series, 2017, p. 226.
[36] Hoek E, Brown ET. Practical estimates of rock mass strength. Int. J. of Rock Mech. and Min. Sci. 1997, 34, 8, pp. 1165-1186. DOI:10.1016/S1365-1609(97)80069-X.
[37] Wilson AH. A method of estimating the closure and strength of lining required in drivages surrounded by a yield zone. Int. J. Rock Mech. Min. Sci. and Geomech. Abstr., 1980, p. 349-355. DOI:10.1016/0148-9062(80)90518-5.
[38] Schullera H, Schweiger HF. Application of a multilaminate model to simulation of shear band formation in NATM-tunnelling. Comput. Geotech. 2002, 29(7): 501–524. DOI: 10.1016/S0266-352X(02)00013-7.
[39] Mortazavi A, Hassani FP, Shabani M. A numerical investigation ofrock pillar failure mechanism in underground openings. Comput. Geotech. 2009, 36(5): 691–697. DOI: 10.1016/j. compgeo.2008.11.004.
[40] Edelbro C. Different approaches for simulating brittle failure in two hard rock mass cases: a parametric study. Rock Mech. Rock Eng., 2010, 43(2):151–165. DOI: 10.1007/s00603-008-0025-x.
[41] Wang SY, Sloan SW, Huang ML, Tang CA. Numerical study of failure mechanism of serial and parallel rock pillars. Rock Mech. Rock Eng., 2011a, 44:179–198. DOI: 10.1007/s00603-010-0116-3.
[42] Wang SL, Zheng H, Li CG, Ge XR. A finite element implementation of strain-softening rock mass. Int. J. Rock Mech. Min. Sci., 2011b, 48:67–76. DOI: 10.1016/j. ijrmms.2010.11.001.